ARMY RESEARCH LABORATORY

Porosity Effects on the Elastic Constants of Five Varieties of Silicon Carbide Ceramic

by Peter Bartkowski and Stephen Spletzer

ARL-TR-2606 November 2001

The findings in this report are not to be construed as an official Department of the Army position unless so designated by other authorized documents.

Citation of manufacturer's or trade names does not constitute an official endorsement or approval of the use thereof.

Destroy this report when it is no longer needed. Do not return it to the originator.

Army Research Laboratory
Aberdeen Proving Ground, MD 21005-5066

ARL-TR-2606 **November 2001**

Porosity Effects on the Elastic Constants of Five Varieties of Silicon Carbide Ceramic

Peter Bartkowski and Stephen Spletzer
Weapons and Materials Research Directorate, ARL

Abstract

Silicon carbide is used in armor applications for its ballistic performance and relative low cost. As such, many types of the material have been developed in an attempt to optimize its properties. The scope of this work encompasses a comparison of the static properties and microstructure of five different silicon carbide materials. Material elastic constants are determined through nondestructive test methods. Elemental composition, microstructure, and porosity effects of the materials are also examined. A model was employed to relate the porosity observed in the microstructure to the determined elastic constants. These results are also compared to a model based on the linear law of mixtures.

Acknowledgments

The authors thank Cliff Hubbard and Jack Mullin of the U.S. Army Research Laboratory, Aberdeen Proving Ground, MD for their assistance in obtaining the micrographs presented in this report.

INTENTIONALLY LEFT BLANK.

Contents

INTENTIONALLY LEFT BLANK.

List of Figures

INTENTIONALLY LEFT BLANK.

List of Tables

INTENTIONALLY LEFT BLANK.

1. Introduction

Considerable research effort has been expended to improve the ballistic properties of armor ceramics. One of the current materials of interest for armor applications is silicon carbide (SiC). As such, many varieties of the ceramic have been developed and tested. To further improve ceramic performance, the effects of microstructure on material properties must be considered.

This work investigates the effects of material microstructure on the elastic constants of SiC ceramics. The elastic constants, elemental composition, and microstructure of five different SiC materials were examined in an effort to determine a relationship between the microstructure and elastic constants. These materials were developed by three separate manufacturers, using three different processing techniques. The reported densities of the materials ranged from 3.137 Mg/m^3 (97.7% dense) to just above that of the crystallographic density of 3.22 Mg/m^3 (Richerson 1992).

2. Materials

SiC materials were obtained from manufacturers in the United States and France. Two varieties were manufactured in the U.S. by CERCOM, Inc. as their SiC-B and SiC-N materials. The third domestically produced material was manufactured by Sohio Corporation. The remaining two materials were obtained from the Société Ceramiques et Composites of France as part of U.S.-France Data Exchange Agreement, DEA-A-95-F-1396 (Riou 1996).

The processing techniques used to manufacture the SiC materials are given in Table 1. Two of the five SiC materials, Sohio, and one of the French, were manufactured using a sintering technique alone. The two CERCOM materials were manufactured by hot pressing (Yamada and Mohri 1991). The other French material was manufactured by a two-step process which consisted of sintering followed by hot isostatic pressing (HIP). Nominal elemental mass compositions were also provided by the manufacturers for each material.

All the materials were manufactured as tiles that ranged from 100 to 150 mm in lateral dimension by 5–25 mm in thickness. Smaller specimens were cut to shape from these tiles with a diamond saw, surface ground flat, and polished on a diamond lapping machine. Specimens were approximately 31.8–40.0 mm in diameter by 6–25 mm in thickness. These specimens were used to examine the material microstructure and measure the mass density and elastic wave speeds.

Table 1. SiC processing techniques and elemental compositions.

Element	Sohio[a]	French Sintered[b]	French Sintered and HIP[b]	CERCOM SiC-B[c]	CERCOM SiC-N[c]
Processing Technique					
	Sintered	Sintered	Sintered & HIPed	Hot Pressed	Hot Pressed
Si	68.51	68.40	68.40	69.50	69.25
C	29.66	30.60	30.60	29.82	29.31
Al	0.03	0.035	0.035	<0.01	1.00
N	0.026	0.37	0.37	0.176	–
Fe	0.02	0.03	0.03	0.30	0.10
O	0.023	0.30	0.30	0.113	–
S	0.024	0.026	0.026	0.027	–
Ti	0.01	0.013	0.013	–	0.04
Zr	0.02	–	–	<0.01	0.03
V	–	–	–	0.02	0.02
Mg	<0.01	0.015	0.015	0.02	–
Ni	–	–	–	–	0.03
Ca	0.02	–	–	–	<0.01
Co	–	–	–	0.02	–
Cr	–	0.006	0.006	–	0.01
Cu	–	0.003	0.003	0.01	–
Na	0.01	–	–	–	–
Hf	–	–	–	0.01	–
P	–	–	–	0.01	–
B	–	–	–	<0.01	–
W	–	<0.01	<0.01	–	–

[a] (Sohio Corporation 1998).
[b] (Riou 1996).
[c] (Chen 1998).

3. Test Procedures/Techniques

Three material properties were needed for the calculation of the SiC elastic constants: mass density, longitudinal wave velocity, and shear wave velocity. Samples were mounted, polished, etched, and examined using a scanning electron microscope (SEM) or metallograph (optical) to obtain photographs of the microstructure.

3.1 Bulk Density

Densities of the samples were determined by using Archimedes' Principle. Dry and wet mass measurements were taken using a Sartorius Micro Balance, which was then applied the buoyancy method for density determination. Specimens were weighed in air at room temperature. An immersion pan carrying the samples was then submerged into a beaker of room temperature deionized water. Using the weight of the specimens in air and in water, along with the temperature dependent density of the water, material densities were calculated by the balance using the relationship described in equation 1 (Sartorius 1995).

$$\rho = \frac{(W_a)(\rho_l)}{W_a - W_l}, \tag{1}$$

where

ρ = sample density,

W_a = sample weight in air,

W_l = sample weight in liquid, and

ρ_l = density of liquid.

Typical sample masses ranged from 25 to 105 g, with the weighing accuracy of the balance rated at ±70 μg. To ensure accurate densities, the system was allowed to stabilize to the nearest μg before any weights were recorded. This system also corrects for buoyancy effects caused by the air. Additionally, several drops of a wetting agent were added to the water to minimize surface tension effects on the immersion pan and reduce the formation of air bubbles. Specimens were also tested for open cell porosity by measuring water absorption. Samples were massed before and after extended submersion (24 hr) in water. Submerged samples were removed from the water, wiped dry, and weighed again. Mass differences were negligible.

For the sample weights used in this report, the systematic uncertainty of the density measurements is negligible. Uncertainties shown for the densities of the SiC materials in this report are due to random variations in the materials.

3.2 Ultrasonic Wave Velocities

Wave velocities were measured using Matec's DSP-8000 software on their MBS-8000 ultrasonic system. Measurements were performed using a pulse-echo (Blitz 1963) noverlay technique. This technique uses a single transducer to send an ultrasonic sound pulse into a sample. The pulse travels into the sample and then reverberates between the front and rear surfaces, creating echoes. These echoes are then captured by the same transducer. The time between echoes is then used in conjunction with the sample thickness to determine the ultrasonic

wave velocity. Since each echo travels through the thickness of the sample twice (down and up) the wave velocity is calculated using the following equation:

$$U = \frac{2 * L}{\Delta t}, \tag{2}$$

where

U = wave velocity,

L = sample thickness, and

Δt = time between echoes.

Sample surfaces were flat and mutually parallel within 15 μm. Transducers were held perpendicular to the sample by a fixture with a 1.5-kg anvil mounted on top of the transducer. Couplant was used between the transducer and sample to improve transmission. Transducer frequencies of 5 and 10 MHz were used for all measurements. Time intervals are accurate to ±0.005 μs.

The accuracy of the system was tested using Z-cut quartz specimens. The measured longitudinal wave velocity was within 0.25% of the known value. The shear wave velocity measurements were within 0.50% of the known value. Shear wave velocities are typically less accurate than longitudinal measurements due to a small phase shift introduced by the couplant. The procedures used for obtaining both longitudinal and shear wave velocities are given in the next section.

3.2.1 Longitudinal Wave Velocity

Longitudinal wave velocities were obtained using a water bath. In this configuration, the transducer is separated from the sample by a water gap which ranged from 4 to 10 mm. The water serves as the couplant. The size of the gap was selected so that the echoes from the sample were clearly separated in time from reverberations in the couplant. This eliminated the phase shift effects caused by thin layers of couplant. A diagram of this configuration is shown in Figure 1.

Figure 2 shows a sample wave train captured from the water bath configuration. The plot shows the wave amplitude vs. time (microsecond). The numbers in Figures 1 and 2 indicate the arrival of the waves at the transducer. The left most pulse (1) is the "main bang,"which is the pulse emitted by the transducer. The next pulse (2) is a reflection from the specimen's top surface. The subsequent smaller amplitude waves (3–5) are reverberating echoes captured from within the specimen. As these echoes have traversed several interfaces of different mechanical impedances, they show a significant reduction in intensity.

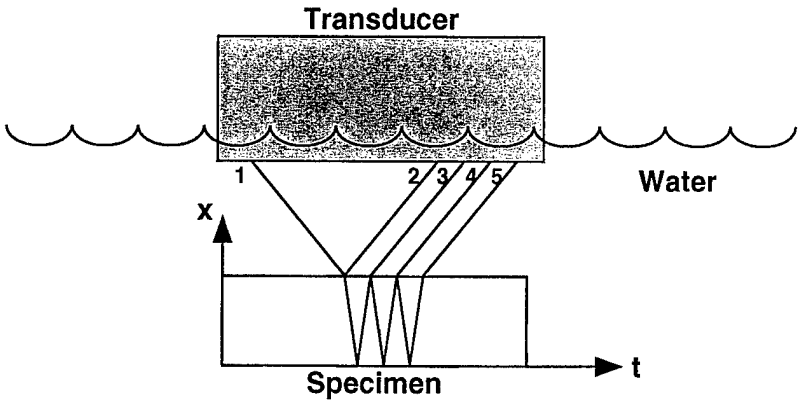

Figure 1. Ultrasonic velocity experimental configuration no. 1.

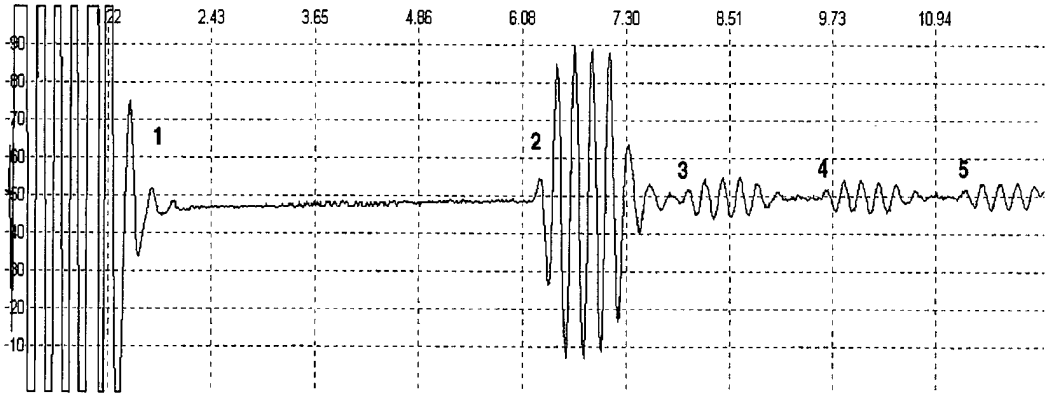

Figure 2. Longitudinal ultrasonic waves as detected by transducer.

3.2.2 Shear Wave Velocity

Shear wave velocities were obtained by coupling the transducer directly to the sample. Although the water bath method used for longitudinal measurements is more accurate, it cannot be used for shear wave velocity measurements, as water will not support a shear wave. A thin layer of honey was used as the couplant. To minimize the phase shift error introduced by the couplant thickness, measurements were taken at least one half hour after the transducer was mounted in place. This allowed the weight of the anvil to squeeze out any excess couplant, thereby enhancing transmission of the waves while minimizing the phase shift error. An example of this configuration is shown in Figure 3.

The wave train shown in Figure 4 was captured during the direct contact shear measurements. As in Figure 2, the first pulse (1) is the main bang. The pulses which follow are echoes (2, 3) from within the specimen. These echoes have a

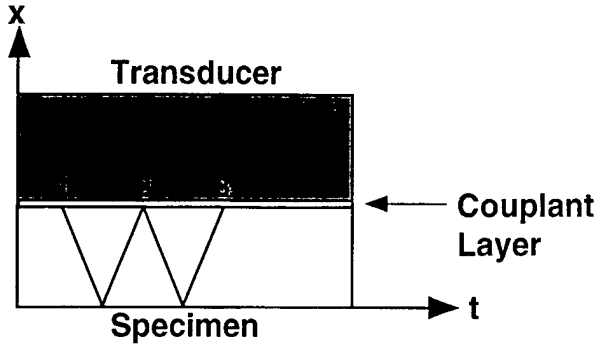

Figure 3. Ultrasonic velocity experimental configuration no. 2.

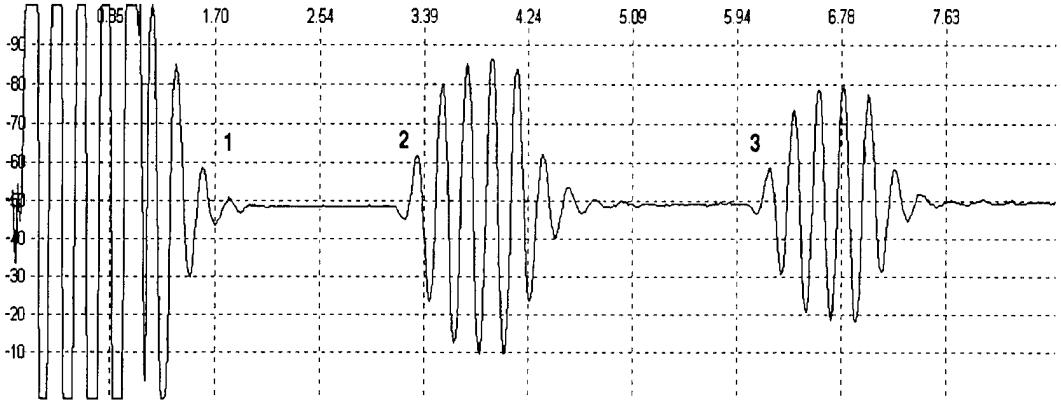

Figure 4. Shear ultrasonic waves as detected by transducer.

much larger intensity than those in Figure 2. This is due to the fact that direct contact between the transducer and specimen increases transmittance due to a closer match of mechanical impedances.

3.3 Microstructure

Information on the microstructure was needed to determine if a relationship could be established between the measured elastic constants and the microstructure as a result of the processing technique. Micrographs were taken of each SiC material to determine grain and pore size. In order to obtain the micrographs, sample specimens were prepared in the following manner.

First, each specimen was mounted in bakelite and placed in a diamond polisher. Specimens were polished to produce an optical finish. Next, the polished specimens were placed in a boiling solution of potassium hydroxide and potassium ferricyanide for 15–20 min. This effectively etched the specimen's

surface, increasing the visibility of the grain boundaries. Specimens were thoroughly cleaned in ethyl alcohol upon their removal from the etchant. Finally, the etched specimens were examined using an SEM or a metallograph (optical). Images of the grain structure were obtained at magnifications of 1000×. Grain and pore sizes were taken as the average of the mean intercept lengths measured from the micrographs.

4. Results and Analysis

4.1 Bulk Density

Densities of the samples were determined using the techniques described earlier in section 3.1, and are listed in Table 2. No mass changes of the samples were observed during extended submersion, indicating no open cell porosity. Bulk mass densities were between 97.7 and 100.2% of the crystallographic density α-SiC(6H) (3.22 Mg/m^3). Densities above this value were observed in all of the CERCOM SiC-N specimens. Individual densities of samples from each material varied by less than 0.13%.

Table 2. Bulk density and elastic wave velocities.

Property	Sohio	French Sintered	French Sintered & HIP	CERCOM SiC-B	CERCOM SiC-N
No. of Samples	4	5	5	8	6
Bulk Density	3.164	3.137	3.184	3.215	3.227
(Mg/m^3)	±0.004	±0.002	±0.004	±0.000	±0.001
U_l (km/s)	12.044	12.055	12.186	12.198	12.262
–	±0.037	±0.031	±0.031	±0.059	±0.031
U_s (km/s)	7.664	7.670	7.730	7.747	7.774
–	±0.042	±0.039	±0.041	±0.054	±0.039

4.2 Elastic Wave Velocities

The results of the ultrasonic measurements are given in Table 2. Wave velocities generally varied proportionately to the density for all the materials. This behavior is evident from the graph in Figure 5, which shows the wave velocities, U_l (longitudinal) and Us (shear) vs. density for all five materials, along with the linear least squares fit line for each wave velocity.

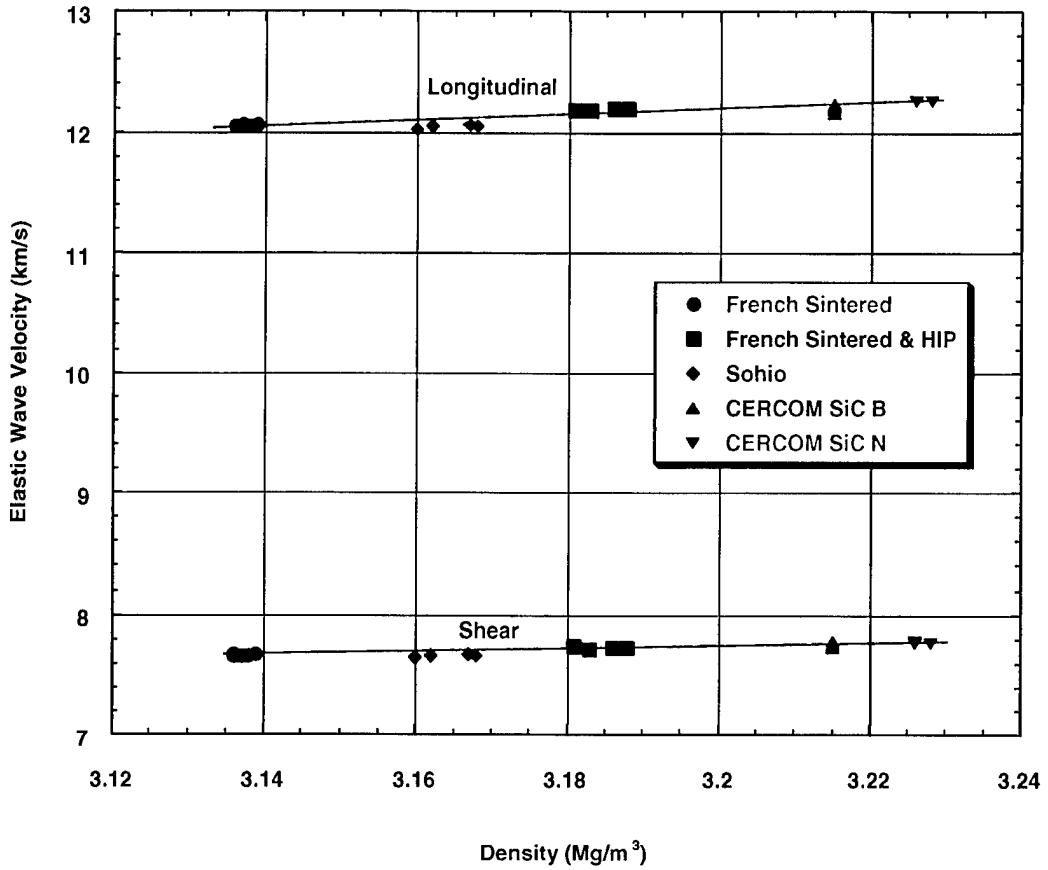

Figure 5. Elastic wave velocities vs. bulk density.

4.3 Elastic Constants

The density and elastic wave velocity measurements were used to determine the elastic constants. All five materials were assumed to be isotropic. Calculations were performed using equations 3–8 (Schreiber et al. 1973), and the results of these equations are shown in Table 3. As expected, the elastic constants varied in a manner similar to the behavior of the wave velocities with respect to density. The elastic constants increased with increases in density and wave speed.

$$L = \rho * U_l^2, \tag{3}$$

$$G = \rho * U_s^2, \tag{4}$$

$$K = \rho * \left(U_l^2 - \left(\frac{4}{3} * U_s^2 \right) \right), \tag{5}$$

Table 3. Elastic constants.

Property	Sohio	French Sintered	French Sintered and HIP	CERCOM SiC-B	CERCOM SiC-N
L	459	456	473	478	485
(GPa)	±3	±3	±3	±5	±3
G	186	185	190	193	195
(GPa)	±2	±2	±2	±3	±2
K	211	210	219	221	225
(GPa)	±6	±5	±5	±8	±5
E	431	428	443	448	454
(GPa)	±35	±31	±33	±49	±32
λ	87	87	92	93	95
(GPa)	±7	±6	±7	±10	±6
ν	0.160	0.160	0.163	0.162	0.164
(-)	±0.015	±0.014	±0.014	±0.022	±0.013

$$E = \rho * \frac{\left(3 * U_l^{\,2} * U_s^{\,2}\right) - \left(4 * U_s^{\,4}\right)}{\left(U_l^{\,2} - U_s^{\,2}\right)}, \tag{6}$$

$$\lambda = \rho * \left(U_l^{\,2} - 2 * U_s^{\,2}\right), \text{ and} \tag{7}$$

$$\upsilon = \frac{U_l^{\,2} - 2U_s^{\,2}}{2 * \left(U_l^{\,2} - U_s^{\,2}\right)}, \tag{8}$$

where

ρ = material density,

K = bulk modulus,

U_l = ultrasonic longitudinal wave velocity,

E = Young's modulus,

U_s = ultrasonic shear wave velocity,

λ = Lamé Constant,

L = Longitudinal Modulus,

υ = Poisson's Ratio, and

G = shear modulus.

4.4 Microstructure

The microstructure of each material was investigated by having samples of each material polished and then chemically etched to show grain boundaries. Micrographs were taken at ×1000. Grain and pore size measurements were taken directly from the micrographs and are listed in Table 4.

Table 4. Material grain sizes.

Material	Grain Size (μm)	Range (μm)	Pore Size (μm)
Sohio	5.4	2–15	3.1
French Sintered	4.1	1–10	3.0
French Sintered and HIP	4.6	1.5–11	3.2
CERCOM SiC-B	5.0	2–10	2.3
CERCOM SiC-N	3.8	1–8	1.9

All the materials exhibited similar microstructural characteristics. Predominant grain sizes were generally around 4–5 μm. This agreed closely with previous studies performed by Riou (1996), which indicated a predominant grain size of 5–6 μm (range of 1–8 μm) for the sintered French material, and Shih et al. (1997) which list an average grain size of 4.1 μm for SiC-B and SiC-N. The Sohio and HIP French materials both have elongated grain structure. In these two materials, the average grain width was 4–5 μm, while grain lengths of 10 μm were common. Pore sizes were generally between 2 and 3 μm in diameter. Pores were smallest, on average, in the two hot pressed materials. Micrographs of each material are shown in Figures 6–10.

4.5 Porosity Effects

All of the materials studied here were between 98 and 99% SiC. However, the bulk densities varied by 3%. This suggested that varying levels of porosity were present in the different materials. Since the sound speeds varied linearly with density, porosity was suspected as being the primary cause for the differences in the elastic constants.

A model was developed by Boccaccini and Fan (1997) to determine the Young's modulus of porous ceramics. This model treats porosity as a zero density second phase. It also assumes that both the material particles and pores are of equiaxed shape and random distribution.

Several parameters were needed to utilize this model. First, the SiC and porosity volume fractions had to be determined from the density measurements using

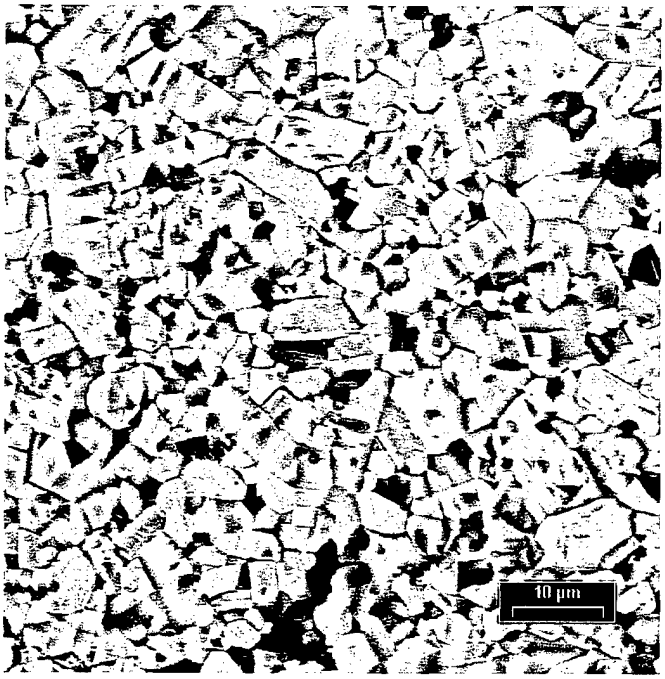

Figure 6. Sohio SiC micrograph (×1000).

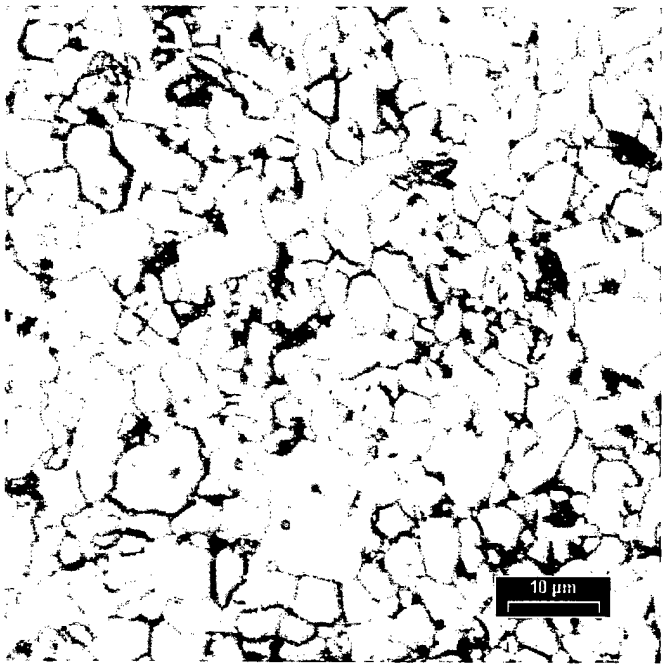

Figure 7. French sintered SiC micrograph (×1000).

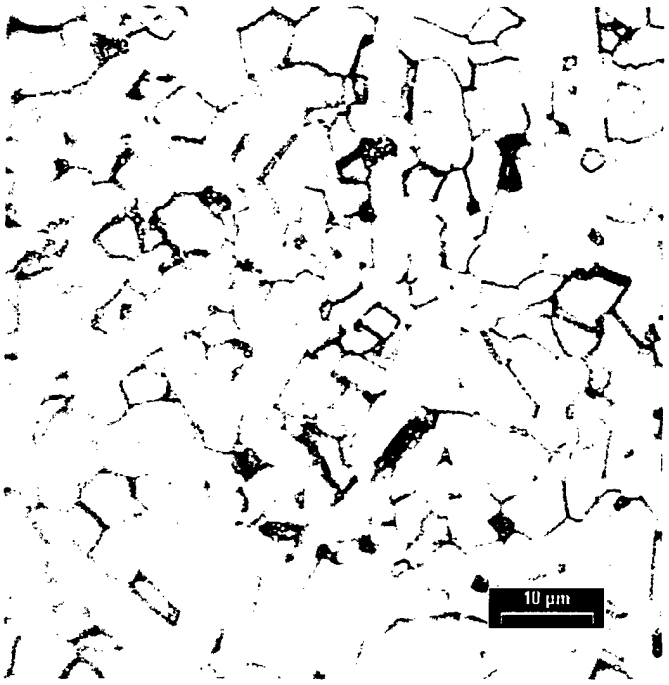

Figure 8. French sintered and HIP SiC micrograph (×1000).

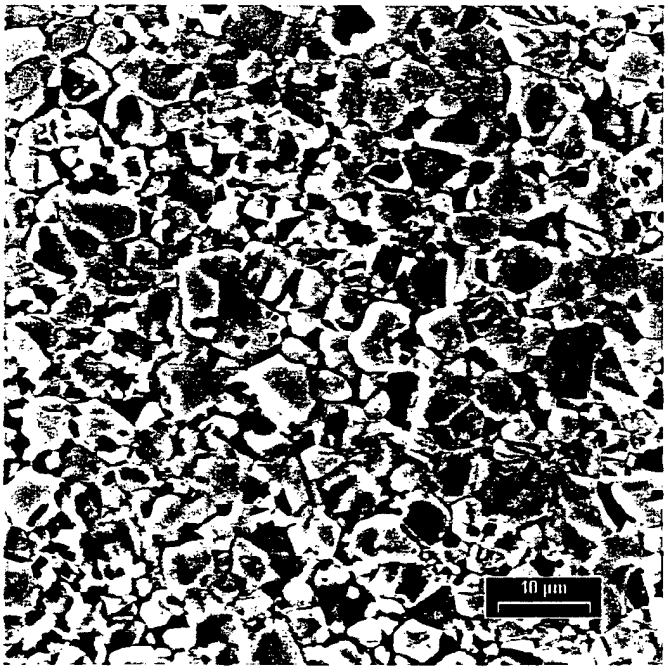

Figure 9. CERCOM SiC-B micrograph (×1000).

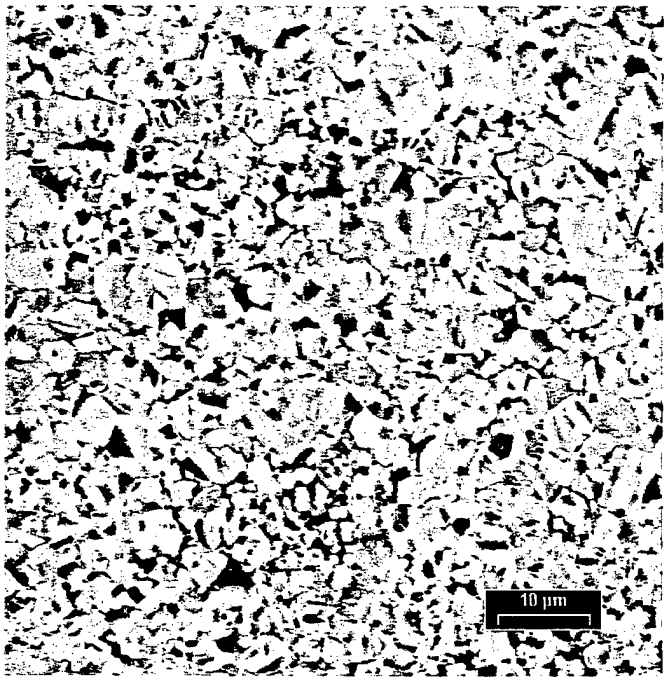

Figure 10. CERCOM SiC-N micrograph (×1000).

equations 9 and 10. Then, the particulate size ratio was calculated using the information obtained from the micrographs (equation 11). Once these values were determined, the continuous volume fraction of the SiC was calculated using equation 12. The effective Young's modulus was then found using equation 13.

If the topological parameters (grain and pore sizes) are unavailable, the power law listed in equation 14 can be used to approximate the continuous volume fraction. The value of the exponent n would be determined through a comparison of the curves generated by this equation to the calculated values of Young's modulus.

$$F_p = 1 - \frac{\rho_{act}}{\rho_{the}}, \tag{9}$$

$$F_m = 1 - F_p = \frac{\rho_{act}}{\rho_{the}}, \tag{10}$$

$$R = \frac{D_p}{D_m}, \tag{11}$$

$$F_c = \frac{F_m^2 R}{F_p + F_m R}, \tag{12}$$

$$E_{eff} = E_m F_c, \text{ and} \tag{13}$$

$$F_c = F_m^n, \tag{14}$$

where

ρ_{act} = measured density,

ρ_{the} = theoretical maximum density,

F_p = porosity volume fraction

F_m = material volume fraction

D_p = pore diameter

D_m = material grain diameter

R = particulate size ratio

F_c = continuous mat. volume fraction

E_m = Material Young's modulus

E_{eff} = Effective Young's modulus

The density of the SiC-N exceeded that of the crystallographic density of SiC by 0.2%. Since variations in the composition of all five materials were slight, with the average Si and C composition at 99%, we assumed all of the materials to be pure SiC. As such, the density and Young's modulus of the SiC-N were used as baseline values for a fully dense SiC material. To simplify the model, we treated all five materials as single phase SiC. As such, the density of the SiC-N was assumed to be the theoretical maximum density.

The results of these calculations are shown in Figure 11 and Table 5. It is evident that the results of the two phase porosity model compare very favorably to the values calculated from the density and elastic wave velocity measurements. Differences between these results are less than 1%. A series of curves were also generated using the power law. An exponent of n = 2.4 adequately models the trend in the modulus of the materials. For comparison, the linear rule of mixtures was also used to predict the Young's modulus behavior. As Figure 11 shows, the linear rule of mixtures failed to accurately predict the moduli of the materials.

Since the results of the porosity model match the values calculated for the Young's modulus from the density and elastic wave velocity measurements, we can conclude that porosity is the primary contributing factor for variations in the elastic constants. A difference of 3% in the densities produced a difference of 6%

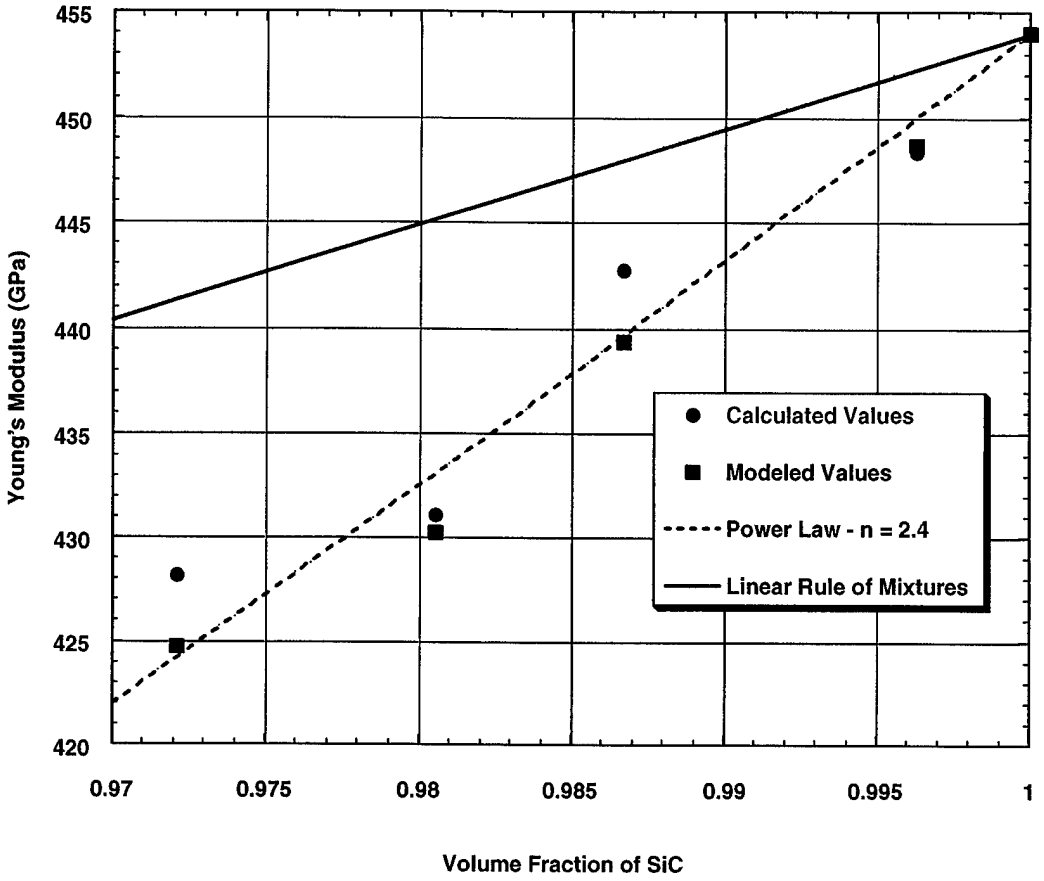

Figure 11. Young's modulus results.

Table 5. Young's modulus results.

Young's Modulus	Sohio	French Sintered	French Sintered and HIP	CERCOM SiC-B	CERCOM SiC-N
Calculated (GPa)	431	428	443	448	454
Porosity Model (GPa)	430	425	439	449	454
Power Law (GPa)	433	424	440	450	454
Linear Law of Mixtures (GPa)	445	441	448	452	454

in the Young's moduli. The remaining elastic moduli can also be predicted using this model, and are listed in Table 6. Poisson's ratio cannot be calculated directly using this model, as it is not density dependent, but can be calculated through elastic constant relations.

Table 6. Modeled elastic moduli.

	Sohio	French Sintered	French Sintered and HIP	CERCOM SiC-B	CERCOM SiC-N
L (GPa)	460	454	469	479	485
G (GPa)	185	182	189	193	195
K (GPa)	213	210	218	222	225
λ (GPa)	90	89	92	94	95

5. Conclusions

Measurement of precise density and wave velocity values demonstrated that all the materials behaved similarly. Wave velocities varied proportionately with density. As density increased, wave velocities and elastic constants followed suit.

Further analysis of the materials through elemental composition and microstructure helped to explain these differences. The five materials were at least 98% SiC, but varied in density from each other by 3%. This suggested that varying levels of porosity were present in these materials.

A model was implemented to determine if porosity was responsible for the differences in the elastic constants of the materials. This model treated porosity as a zero density, second phase material. Using the grain and pore sizes taken from the micrographs, an effective Young's modulus was calculated for each material. The results of this model agree well with the values calculated from the bulk density and sound speed measurements. As such, porosity effects are considered to be the primary cause of the variations in the elastic constants.

In conclusion, the elastic behaviors of all of the materials were very similar. The differences seen between these relatively pure materials can be attributed to porosity effects created by the processing techniques. The two hot pressed materials had the highest densities, smallest pore sizes, and therefore the highest values for the elastic moduli.

6. References

Blitz, J. *Fundamentals of Ultrasonics.* Butterworth & Co., 1963.

Boccaccini, A. R., and Z. Fan. "A New Approach for the Young's Modulus-Porosity Correlation of Ceramic Materials." *Ceramic International* 23, pp. 239–245, 1997.

Chen, B. Personal communication. CERCOM Inc., Vista, CA, 1998.

Richerson, D. W. *Modern Ceramic Engineering, Properties, Processing, and Use in Design.* New York: Marcel Dekker, 1992.

Riou, P. "Study of the Damage of Silicon Carbide at Low Energy Impact, Impact: Application to Armor." Ph.D. Thesis, L'Ecole Nationale Superieure des Mines de Paris, 1996.

Sartorius Co. *Sartorius Microbalance MC210P Manual.* Goettingen, Germany: Sartorius AG, 1995.

Schreiber, E., L. O. L. Anderson, and N. Soga. "The Elastic Moduli." *Elastic Constants and Their Measurements,* McGraw-Hill, 1973.

Shih, C. J., V. F. Nesterenko, and M. A. Meyers. "High-Strain-Rate and Comminution of Silicon Carbide." *Acta Materialia,* 1997.

Sohio Corporation. Personal communication. 1998.

Yamada, K., and M. Mohri. "Properties and Applications of Silicon Carbide Ceramics." *Silicon Carbide Ceramics,* edited by S. Somiya and Y. Inomata, New York: Elsevier Applied Sciences Publishing, 1991.

INTENTIONALLY LEFT BLANK.

NO. OF COPIES	ORGANIZATION
2	DEFENSE TECHNICAL INFORMATION CENTER DTIC OCA 8725 JOHN J KINGMAN RD STE 0944 FT BELVOIR VA 22060-6218
1	HQDA DAMO FDT 400 ARMY PENTAGON WASHINGTON DC 20310-0460
1	OSD OUSD(A&T)/ODDR&E(R) DR R J TREW 3800 DEFENSE PENTAGON WASHINGTON DC 20301-3800
1	COMMANDING GENERAL US ARMY MATERIEL CMD AMCRDA TF 5001 EISENHOWER AVE ALEXANDRIA VA 22333-0001
1	INST FOR ADVNCD TCHNLGY THE UNIV OF TEXAS AT AUSTIN 3925 W BRAKER LN STE 400 AUSTIN TX 78759-5316
1	US MILITARY ACADEMY MATH SCI CTR EXCELLENCE MADN MATH THAYER HALL WEST POINT NY 10996-1786
1	DIRECTOR US ARMY RESEARCH LAB AMSRL D DR D SMITH 2800 POWDER MILL RD ADELPHI MD 20783-1197
1	DIRECTOR US ARMY RESEARCH LAB AMSRL CI AI R 2800 POWDER MILL RD ADELPHI MD 20783-1197

NO. OF COPIES	ORGANIZATION
3	DIRECTOR US ARMY RESEARCH LAB AMSRL CI LL 2800 POWDER MILL RD ADELPHI MD 20783-1197
3	DIRECTOR US ARMY RESEARCH LAB AMSRL CI IS T 2800 POWDER MILL RD ADELPHI MD 20783-1197
	ABERDEEN PROVING GROUND
2	DIR USARL AMSRL CI LP (BLDG 305)

NO. OF COPIES	ORGANIZATION
1	CECOM SP & TRRSTRL COMMCTN DIV AMSEL RD ST MC M H SOICHER FT MONMOUTH NJ 07703-5203
1	PRIN DPTY FOR TCHNLGY HQ US ARMY MATCOM AMCDCGT R PRICE 5001 EISENHOWER AVE ALEXANDRIA VA 22333-0001
1	PRIN DPTY FOR ACQUSTN HQS US ARMY MATCOM AMCDCGA D ADAMS 5001 EISENHOWER AVE ALEXANDRIA VA 22333-00001
1	DPTY CG FOR RDE HQS US ARMY MATCOM AMCRD 5001 EISENHOWER AVE ALEXANDRIA VA 22333-00001
1	ASST DPTY CG FOR RDE HQS US ARMY MATCOM AMCRD COL S MANESS 5001 EISENHOWER AVE ALEXANDRIA VA 22333-00001
3	AIR FORCE ARMAMENT LAB AFATL DLJW W COOK D BELK J FOSTER EGLIN AFB FL 32542
1	DPTY ASSIST SCY FOR R & T SARD TT THE PENTAGON RM 3E479 WASHINGTON DC 20310-0103
1	DARPA L STOTTS 3701 N FAIRFAX DR ARLINGTON VA 22203-1714

NO. OF COPIES	ORGANIZATION
1	DIRECTOR US ARMY RESEARCH LAB AMSRL CS AL TA 2800 POWDER MILL ROAD ADELPHI MD 20783-1145
3	DIRECTOR US ARMY ARDEC AMSTA AR FSA E W P DUNN J PEARSON E BAKER PICATINNY ARSENAL NJ 07806-5000
2	US ARMY TARDEC K BISHNOI D TEMPLETON AMSTRA TR R MS 263 WARREN MI 48397-5000
4	COMMANDER US ARMY BELVOIR RD&E CTR STRBE N WESTLICH STRBE NAN S G BISHOP J WILLIAMS FORT BELVOIR VA 22060-5166
1	COMMANDER US ARMY RESEARCH OFFICE A RAJENDRAN PO BOX 12211 RESEARCH TRIANGLE PARK NC 27709-2211
1	NAVAL RESEARCH LAB A E WILLIAMS CODE 6684 4555 OVERLOOK AVE SW WASHINGTON DC 20375

NO. OF COPIES	ORGANIZATION
10	DIRECTOR SANDIA NATL LABS E S HERTEL JR MS 0819 J ASAY MS 1811 R BRANNON MS 0820 L CHHABILDAS MS 1811 D CRAWFORD MS 0821 M FURNISH MS 0821 P TAYLOR ORG 1432 M KIPP MS 0820 P YARRINGTON MS 0820 M FORRESTAL DIV 1551 PO BOX 5800 ALBUQUERQUE NM 87185-0307
10	DIRECTOR LLNL M J MURPHY J AKELLA N C HOLMES W TAO L282 J FORBES P URTIEW L282 A HOLT L290 J E REAUGH L290 W J NELLIS L299 J B CHASE L099 PO BOX 808 LIVERMORE CA 94550
7	DIRECTOR LANL D MANDELL P MAUDLIN R GRAY J SHANER MS F670 R DAVIDSON MS K557 J JOHNSON G787 F ADDESSIO G787 PO BOX 1663 LOS ALAMOS NM 87545
3	CALTECH A INGERSOLL MS 170 25 PROF G RAVICHANDRAN T J AHRENS MS 252 21 1201 E CALIFORNIA BLVD PASADENA CA 91125

NO. OF COPIES	ORGANIZATION
1	ARMY HIGH PERFORMANCE COMPUTING RSRCH CTR T HOLMQUIST 1200 WASHINGTON AVENUE S MINNEAPOLIS MN 55415
2	SOUTHWEST RESEARCH INSTITUTE C ANDERSON J WALKER P O DRAWER 28510 SAN ANTONIO TX 78284
2	UNIVERSITY OF DELAWARE DEPT OF MECH ENGINEERING PROF J GILLESPIE PROF J VINSON NEWARK DE 19716
3	SRI INTERNATIONAL D CURRAN D SHOCKEY R KLOPP 333 RAVENSWOOD AVENUE MENLO PARK CA 94025
1	VIRGINIA POLYTECHNIC INST COLLEGE OF ENGINEERING R BATRA BLACKSBURG VA 24061-0219
1	ALLIANT TECHSYSTEMS INC GR JOHNSON MN11 1614 600 SECOND ST NE HOPKINS MN 55343
1	COMPUTATIONAL MECHANICS CONSULTANTS J A ZUKAS P O BOX 11314 BALTIMORE MD 21239-0314
1	KAMAN SCIENCES CORP D L JONES 2560 HUNTINGTON AVE SUITE 200 ALEXANDRIA VA 22303

NO. OF COPIES	ORGANIZATION
9	INST OF ADVANCED TECH UNIVERSITY OF TX AUSTIN S BLESS J CAZAMIAS H FAIR D LITTLEFIELD I MCNAB C PERSAD W REINECKE P SULLIVAN S SATAPATHY 3925 W BRAKER LANE SUITE 400 AUSTIN TX 78759-5316
1	APPLIED RESEARCH ASSOCIATES D E GRADY 4300 SAN MATEO BLVD NE SUITE A220 ALBUQUERQUE NM 87110
1	INTERNATIONAL RESEARCH ASSOCIATES INC D L ORPHAL 4450 BLACK AVE PLEASANTON CA 94566
1	JET PROPULSION LABORATORY M ADAMS IMPACT PHYSICS GROUP 4800 OAK GROVE DRIVE PASADENA CA 91109
1	THE DOW CHEMICAL CO M EL RAHEB CENTRAL RSRCH ENGINEERING LABORATORY BUILDING 1776 MIDLAND MI 48640
1	BOB SKAGGS CONSULTANT S R SKAGGS 79 COUNTY RD 117 SOUTH SANTA FE NM 87501
1	WASHINGTON ST UNIVERSITY SCHOOL OF MECHANCIAL AND MATERIAL ENGINEERING J L DING PULLMAN WA 99164-2920

NO. OF COPIES	ORGANIZATION
1	WASHINGTON ST UNIVERSITY INSTITUTE OF SHOCK PHYSIC Y M GUPTA PULLMAN WA 99164-2814
1	COORS CERMANIC COMPANY T RILEY 600 NINTH STREET GOLDEN CO 80401
1	ARIZONA STATE UNIVERSITY MECHANICAL AND AEROSPACE ENGINEERING D KRAVCINOVIC TEMPE AZ 85287-6106
1	UNIVERSITY OF DAYTON RESEARCH INSTITUTE C HARI SIMHA MS SPC 1911 300 COLLEGE PARK DAYTON OH 45469
5	DIRECTOR USARL K WILSON (5 CPS) FRENCH DEA 1396 ADELPHI MD 20783-1197

NO. OF
COPIES ORGANIZATION

ABERDEEN PROVING GROUND

38 DIR USARL
AMSRL WM
E SCHMIDT
T WRIGHT
AMSRL WM TA
T HAVEL
M NORMANDIA
W A GOOCH
P BARTKOWSKI (10)
H W MEYER
E HORWATH
AMSRL WM TC
K KIMSEY
D SCHEFFLER
R COATES
AMSRL WM MB
G GAZONAS
AMSRL SL BE
A PRAKASH
AMSRL WM TD
A M DIETRICH
M RAFTENBERG
M SCHEIDLER
E RAPACKI
J M BOTELER
T WEERASOORIYA
D GROVE
D DANDEKAR (10)

NO. OF COPIES	ORGANIZATION
1	DERA N J LYNCH WEAPONS SYSTEMS BUILDING A20 DRA FORT HALSTEAD SEVENOAKS KENT TN 147BP UNITED KINGDOM
2	ERNST MACH INTITUT VOLKER HOHLER H NAHAME ECKERSTRASSE 4 D-7800 FREIBURG 1 BR 791 4 GERMANY
1	FOA2 P LUNDBERG S-14725 TUMBA SWEDEN
1	PCS GROUP CAVENDISH LABORATORY W G PROUD MADINGLEY RD CAMBRIDGE UNITED KINGDOM
1	CENTRE D'ETUDES DE GRAMAT J Y TRANCHET 46500 GRAMAT FRANCE
1	MINISTERE DE LA DEFENSE DR G BRAULT DGA/DSP/STTC 4 RUE DE LA PORTE D'ISSY 75015 PARIS FRANCE
1	SPART DIRECTION - BP 19 DR E WARINGHAM 10 PLACE GEORGES CLEMENCEOUX 92211 SAINT CLOUD CEDEX FRANCE
1	ROYAL MILITARY COLLEGE OF SCIENCE CRANEFIELD UNIVERSITY PROF N BOURNE SHRIVENHAM SWINDON SN6 8LA UNITED KINGDOM

REPORT DOCUMENTATION PAGE

Form Approved
OMB No. 0704-0188

1. AGENCY USE ONLY *(Leave blank)*	2. REPORT DATE	3. REPORT TYPE AND DATES COVERED
	November 2001	Final, February 1998–December 1999

4. TITLE AND SUBTITLE
Porosity Effects on the Elastic Constants of Five Varieties of Silicon Carbide Ceramic

5. FUNDING NUMBERS
0602105AH84

6. AUTHOR(S)
Peter Bartkowski and Stephen Spletzer

7. PERFORMING ORGANIZATION NAME(S) AND ADDRESS(ES)
U.S. Army Research Laboratory
ATTN: AMSRL-WM-TA
Aberdeen Proving Ground, MD 21005-5066

8. PERFORMING ORGANIZATION REPORT NUMBER
ARL-TR-2606

9. SPONSORING/MONITORING AGENCY NAMES(S) AND ADDRESS(ES)

10.SPONSORING/MONITORING AGENCY REPORT NUMBER

11. SUPPLEMENTARY NOTES

12a. DISTRIBUTION/AVAILABILITY STATEMENT
Approved for public release; distribution is unlimited.

12b. DISTRIBUTION CODE

13. ABSTRACT*(Maximum 200 words)*

Silicon carbide is used in armor applications for its ballistic performance and relative low cost. As such, many types of the material have been developed in an attempt to optimize its properties. The scope of this work encompasses a comparison of the static properties and microstructure of five different silicon carbide materials. Material elastic constants are determined through nondestructive test methods. Elemental composition, microstructure, and porosity effects of the materials are also examined. A model was employed to relate the porosity observed in the microstructure to the determined elastic constants. These results are also compared to a model based on the linear law of mixtures.

14. SUBJECT TERMS
elastic constants, porosity, silicon carbide

15. NUMBER OF PAGES
30

16. PRICE CODE

17. SECURITY CLASSIFICATION OF REPORT	18. SECURITY CLASSIFICATION OF THIS PAGE	19. SECURITY CLASSIFICATION OF ABSTRACT	20. LIMITATION OF ABSTRACT
UNCLASSIFIED	UNCLASSIFIED	UNCLASSIFIED	UL

INTENTIONALLY LEFT BLANK.